Neutronics analysis and activation calculation for Tungsten used in the DEMO divertor targets: A comparative study between the effects of WCLL and HCPB blanket, different W compositions and Chromium

Simone Noce[a], Davide Flammini[b], Giovanni Mariano[b,c], Giuseppe Mazzone[b], Fabio Moro[b], Francesco Romanelli[a], Rosaria Villari[b], Jeong-Ha You[d]

[a]*University of Rome Tor Vergata, Industrial Engineering Department, via del Politecnico 1, 00133, Rome, Italy*
[b]*ENEA FSN-FUSTEC-TEN, C.R. Frascati, via E. Fermi 45, 00044 Frascati (Rome), Italy*
[c]*DIAEE, Sapienza University of Rome, Corso Vittorio Emanuele II, 244, 00186 Rome, Italy*
[d]*Max-Planck-Institut für Plasmaphysik, Boltzmannstrasse 2, 85748 Garching, Germany*

The Divertor Plasma Facing Components (PFCs) of a fusion reactor play a key role in the removal of plasma power exhaust and impurity particles, being exposed to very intense thermal load and high neutron irradiation, which can severely compromise their functioning capability. Therefore, the choice of the plasma facing materials (PFMs) is a fundamental aspect in the design of these components. Tungsten is presently the main candidate being characterised by several advantages from a thermo-physical point of view, but also some drawbacks (e.g. significant activation under neutron irradiation). Neutronics assessment plays a key role in the design of these critical components and in the choice of the most suitable PFMs. Detailed nuclear analyses have been performed by implementing, for the first time, heterogeneous models of the actual ITER-Like PFCs geometry [1][2], aimed to assess the impact of neutronics and activation issues on design, lifetime, operations and safety of the PFCs of DEMO divertor and to provide outcomes useful in the PFCs selection concept, under study within the EUROfusion WPDIV-2 project. In particular way, the effects of two different blankets (WCLL and HCPB) on W activation and the impact of three different W compositions and chromium, have been compared. Three-dimensional neutronic analyses have been performed with the MCNP5 Monte Carlo [3] using the reference JEFF 3.3 nuclear data libraries [4] to calculate neutron spectra in PFCs subcomponents. Activation analysis has been performed with FISPACT II inventory codes [5] to assess the specific activity, decay heat and contact dose at the end of DEMO-1 operations. The calculations have been carried-out on ENEA HPC CRESCO6 cluster [6].

Keywords: PFC, DEMO, neutronics, Divertor, MCNP

1. Introduction

One of the most fundamental missions of the recent European roadmap drafted for realizing commercially viable fusion power generation, is the reliable power handling [7][8]. In this regard, the divertor is the key in-vessel component, as it is responsible for power exhaust and impurity removal via guided plasma exhaust [9]. Due to the intense bombardment of energetic plasma particles, the Plasma-Facing Components (PFCs) of the divertor are exposed to extreme heat flux loads [10]. The divertor is besides subjected to significant neutron irradiation, being directly facing to the reaction chamber. The evaluation of neutronics loads is essential for the design of its components, especially for the targets, whose operating conditions are among the most critical [11][12]. Therefore, the choice of the first wall materials plays a crucial role for the functioning and lifetime of the PFCs. It is required the use of materials with an extremely high melting point combined with a suitable room temperature thermal conductivity. Essential requirements are also a sufficient resistance to thermo-mechanical stress, as well as a low tendency to activation induced by neutron irradiation, and preserving their properties under these critical operating conditions. Tungsten fulfills most of these requisites, appearing to be the most attractive material candidate for high heat flux components, from a thermo-physical point of view. On the other side, it shows a brittle nature and a strong tendency to recrystallize at high temperatures well below the melting point. Moreover, tungsten is subjected to a significant induced activation by neutrons [13]. Chromium is another interesting PFM candidate, especially due to its low activation behaviour, under neutron exposure. The use of chromium as Low Activation Material (LAM) [14] to realize the PFC tiles leads to a reduction of radioactive inventory in a fusion reactor, that means: a reduction of waste disposal and decommissioning problems, an easier maintenance [15]. According to what has been stated, it is evident how performing an in-depth analysis on the induced activation of tungsten and other possible candidates, represents a pivotal step in the design and selection of the PFCs concepts. The PFCs of a divertor cassette consists of three parts, namely, straight leg of the vertical target, liner and reflector plates (replaced by the dome in some previous configurations) and baffle region [16]. The 2019 DEMO divertor cassette layout is shown in figure 1 [17]. This work is focused on an extensive neutronics and activation comparative analysis mainly concerning the tungsten used for the DEMO divertor targets. In particular way, this study consists of the following parts:

- Comparison between the effects of the WCLL and HCPB blanket on the W activation

author's email: Simone.Noce@uniroma2.it

behaviour (specific activity, contact dose rate and decay heat).

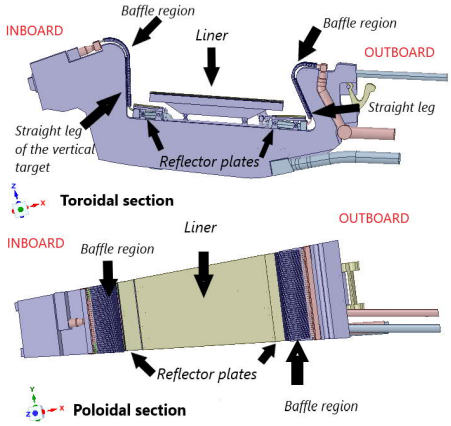

Figure 1. Latest neutronics CAD model of the DEMO divertor cassette body 2019 [26].

- Assessment of the concentration of the principal transmutation products of tungsten [18] and copper [19] with comparison between the WCLL and HCPB blanket case.
- Comparison between chromium and different three tungsten compositions (two primary candidates and the reference W composition [18], recommended for the neutronics analyses), in terms of specific activity, contact dose rate and decay heat.

Two MCNP models have been reproduced: WCLL [20][21][22] and HCPB [23] Single Module Segment layered blankets, both with the new MCNP model of the divertor 2019 configuration. Detailed MCNP representations of the whole ITER-Like (IL) PFCs inner and outer targets have been recreated and integrated in both the above-mentioned models. Neutron and gamma transport simulations have been performed using MCNP5v1.6 Monte Carlo code [3] and the Joint Evaluated Fusion File JEFF 3.3 nuclear data libraries [4]. Activation analyses have been carried out by means of FISPACT II inventory code [5] and TENDL 2015 [24] libraries.

2. Blanket and Divertor PFCs MCNP models description and integration

The analyses have been performed using two models: starting from the EU DEMO1 2017 reference configuration MCNP model (representing a 11.25° toroidal sector of the tokamak, with plasma parameters shown in table 1) [25] two MCNP geometrical models with semi-heterogeneous blanket representation of WCLL and HCPB blanket, both with the MCNP model of the divertor 2019 configuration [17], have been generated (figure 2). Moreover, the detailed MCNP model of the entire ITER-Like PFCs targets (CAD model [26] shown in figure 3) have been reproduced and integrated in the WCLL and HCPB model (figure 4). Each IL monoblock is made of tungsten and it's 28 mm high, 23 mm wide and 12 mm thick. It is crossed by a CuCrZr cooling pipe with internal and external diameter of 12 and 15 mm respectively. These two components are separated by 1 mm thick pure copper interlayer. The minimum distance between the interlayer outer surface and the three side walls of the monoblock is 3 mm while the distance from the monoblock upper surface is 8 mm (figure 5).

Table 1. Main parameters of the DEMO baseline configuration.

N° of Toroidal Field Coils	16
Major radius (m)	8.938
Minor radius (m)	2.883
Aspect ratio	3.1
Plasma elongation	1.65
Plasma triangularity	0.33
Fusion power (MW)	1998
Average neutron wall loading (MW/m^2)	1.04
Net electric power (MW)	500

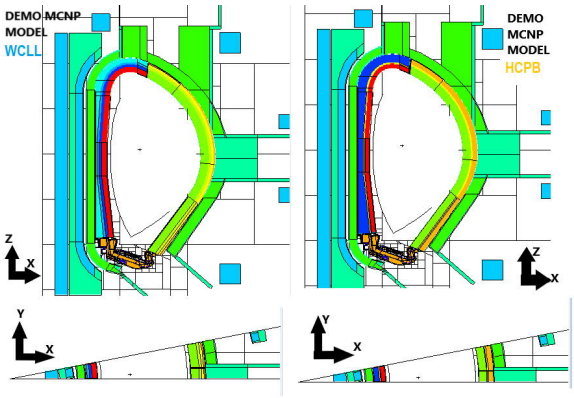

Figure 2. WCLL (left) and HCPB (right) DEMO single module semi-heterogeneous MCNP models, with divertor 2019 cassette body [17].

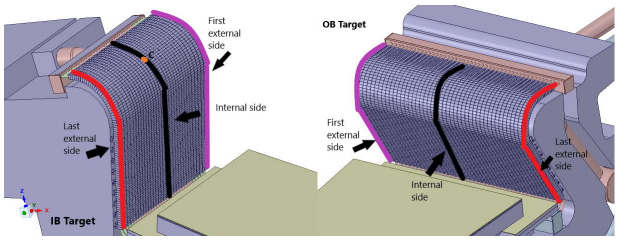

Figure 3. Inboard (left) and outboard (right) targets (CAD model [26]), in which are highlighted the external sides, the innermost side with the point C on the inboard baffle region.

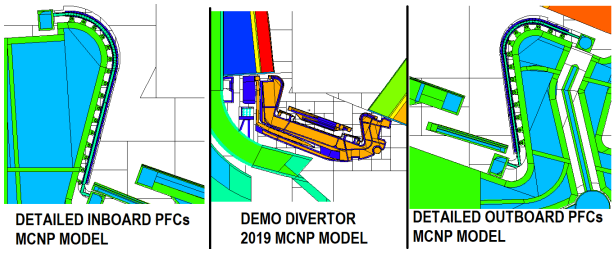

Figure 4 Heterogeneous divertor 2019 cassette body model (central), detailed IL PFCs inboard (left) and outboard (right) targets representation (toroidal view).

The PFC-CB supports have been modeled in details as shown in figures 4 and 6. The pre-processing and preparation of the IL CAD model has been performed by means of the 3D modeling software Ansys SpaceClaim 2019 [27] in order to generate a CAD model suitable for neutronic analyses. The simplified CAD model has been

converted into the equivalent MCNP geometrical representation using the CAD-to-MCNP interface of SuperMC [28].

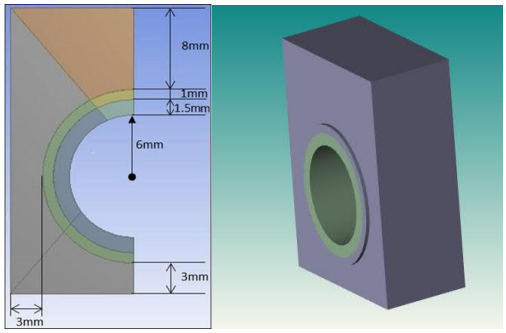

Figure 5. Geometrical description of the ITER-Like PFC concept [1,2].

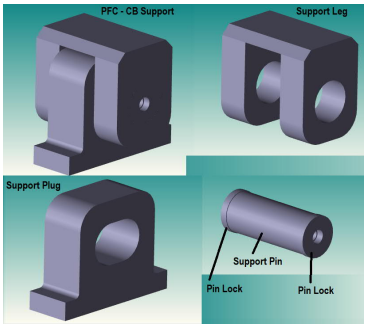

Figure 6. Geometrical description of the PFC-CB Support sub-components (leg, plug, pin and pin locks) [26].

To create a correct coupling between the neutronics model of the PFC and that of the cassette body and to simplify the model integration phase, it has been necessary to integrate 31 (inboard) and 43 (outboard) CuCrZr pipes in the DEMO divertor 2019 MCNP model, which is shown in figure 4. On each pipe can be arranged 78 and 70 W-monoblocks and the corresponding Cu-interlayers, on inboard and outboard respectively. Regarding the PFC-CB support design, in these models has been integrated 16 and 14 PFCs-CB supports on inboard and outboard respectively, for each CuCrZr pipe. It should be noted that the arrangement of the supports in the baffle region has not been reported in the reference divertor CAD model [26], therefore it has been assumed to be the same as that on the straight leg. A slightly more simplified configuration consisting of support leg, support plug, pin and pin locks has been implemented, following the reference geometry reported in the CAD [26]. There aren't alumina components (needed for the electrical insulation), for which it has been however possible to evaluate the maximum neutronics loads values (in the central zone of the targets), in the previous studies [29]. The WCLL Breeding Blanket (BB) model is based on layered configuration along the radial direction representing the internal blanket structure: First Wall and Side Wall (FW-SW) and W-armour, Breeding Zone (BZ), LiPb and Water manifolds, Back Supporting Structure (BSS). The radial layout subdivision of the breeding unit is shown in figure 7 and the corresponding material mixtures for each layer are shown in tables 2 and 3. The materials properties and composition have been selected according to the specifications for neutronic analyses in the EUROfusion framework [18].

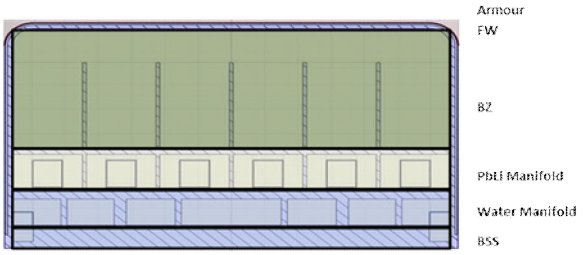

Figure 7. WCLL DEMO semi-heterogeneous blanket layers subdivision (toroidal view), in which are highlighted W-Armour, First Wall and Side Wall (FW-SW), Breeding Zone (BZ), PbLi and Water manifolds and Back Supporting Structure (BSS).

Table 2. WCLL semi-heterogeneous outboard layer subdivision and materials mixtures compositions.

Outboard	Radial thickness (mm)	W vol %	Water vol %	LiPb vol %	Eurofer vol %
Armour	2	100.00%	0.00%	0.00%	0.00%
FW-SW	25	0.00%	6.09%	0.00%	93.91%
BZ	538	0.00%	1.41%	87.63%	10.96%
PbLi Manifold	174	0.00%	1.13%	79.69%	19.18%
Water Manifold	155	0.00%	64.31%	0.00%	35.69%
BSS	100	0.00%	4.97%	0.00%	95.03%

Table 3. WCLL semi-heterogeneous inboard layer subdivision and materials mixtures compositions.

Inboard	Radial thickness (mm)	W vol %	Water vol %	LiPb vol %	Eurofer vol %
Armour	2	100.00%	0.00%	0.00%	0.00%
FW-SW	25	0.00%	6.77%	0.00%	93.23%
BZ	330.2	0.00%	1.18%	86.90%	11.92%
PbLi Manifold	174	0.00%	1.20%	80.06%	18.73%
Water Manifold	155	0.00%	64.14%	0.00%	35.86%
BSS	100	0.00%	5.54%	0.00%	94.46%

Taking into account the complexity of the breeding blanket internal structure and component assembly (detailed description shown in figure 8), also the HCPB BB MCNP modelling approach has been based on the segmentation of the BB radial layers with specifically defined material mixtures [23], which are shown in tables 4 and 5. It's well to stress that the water cooled blanket uses the liquid Lithium-Lead (LiPb, 84.2 atomic percent Pb, 15.8 atomic percent Li) with 6Li enriched to 90% as breeder, neutron multiplier and tritium carrier. In the helium cooled blanket, a mixture Li4SiO4 + 35% mol Li2TiO3 (KALOS CB, 6Li enriched to 60%) and Be12Ti [23][30][31], are utilized, as tritium breeder and neutron multiplier respectively.

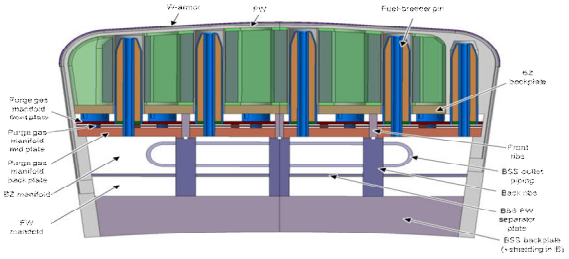

Figure 8. HCPB DEMO blanket internal layout (toroidal view) [23].

Table 4. HCPB semi-heterogeneous layer repartition and materials mixtures compositions for outboard [23].

Outboard	Radial thickness (mm)	W vol %	Be12Ti vol %	KALOS CB vol %	Eurofer vol %	Void (He) vol%
Armour	2	100.00 %	0.00%	0.00%	0.00%	0.00%
FW-SW	20.08	0.00%	0.00%	0.00%	57.30 %	42.70 %
BZ	511.9	0.00%	49.30 %	10.30 %	14.30 %	26.10 %
Back-plate	30	0.00%	0.00%	10.80 %	80.20 %	9.00%
Outlet plenum + purge gas manifolds	88	0.00%	0.00%	6.10%	37.90 %	56.00 %
BSS manifold	342.06	0.00%	0.00%	1.20%	46.70 %	52.100 %
Caps	30	0.00%	0.00%	5.40%	89.00 %	5.60%

Table 5. HCPB semi-heterogeneous layer repartition and materials mixtures compositions for inboard [23].

Inboard	Radial thickness (mm)	W vol %	Be12Ti vol %	KALOS CB vol %	Eurofer vol %	Void (He) vol%
Armour	2	100.00 %	0.00%	0.00%	0.00%	0.00%
FW-SW	20.08	0.00%	0.00%	0.00%	68.20 %	31.80 %
BZ	283.3	0.00%	55.50 %	8.80%	12.30 %	23.40 %
Back-plate	30	0.00%	0.00%	10.80 %	80.20 %	9.00%
Outlet plenum + purge gas manifolds	88	0.00%	0.00%	6.10%	37.90 %	56.00 %
BSS manifold	342.06	0.00%	0.00%	1.20%	66.40 %	32.40 %
Caps	30	0.00%	0.00%	5.40%	89.00 %	5.60%

3. Nuclear analyses

The activation results (specific activity, dose rate, decay heat) on tungsten [18] monoblocks are presented in terms of inboard (IB) and outboard (OB) profiles along the divertor poloidal abscissa (figure 9), considering HCPB and WCLL blanket and for different cooling times after plasma shutdown (starting time, 1 year, 50 years). The W-Monoblocks placed on the external side of the targets (figure 3, highlighted in red) have been considered, where the neutron fluxes are generally more intense (due to the backscatter and streaming neutrons between one CB and another). Peak concentrations of main transmutation products of tungsten and copper have been evaluated both for WCLL and HCPB, comparing them.

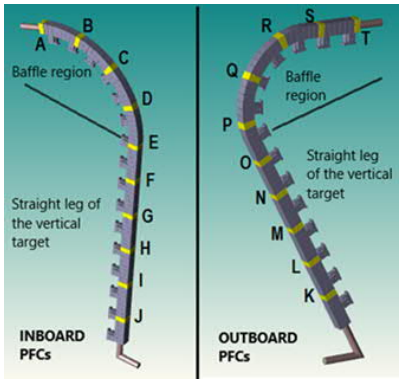

Figure 9. Single units of CuCrZr pipe (inboard and outboard) with W-Monoblocks, Cu-Interlayers and supports, in which are highlighted the W-Monoblocks positions, chosen for the evaluation of the poloidal profiles.

Furthermore, comparison between different tungsten compositions (reference for the neutronics analyses [18] and AT&M Chinese company [19], A.L.M.T. corp. Japanese company [32], batch specification from supplier) and chromium (made by Plansee company [33]), has been done, in terms of time profiles of specific activity, contact dose rate and decay heat after plasma shutdown. For a better comprehension, the detailed specifications and chemical compositions of the above-mentioned materials, are shown from table 6 to 10. In this case, the evaluation has been carried out on the monoblock C placed in the central zone of the inboard baffle region (figure 3), and considering only the WCLL blanket case.

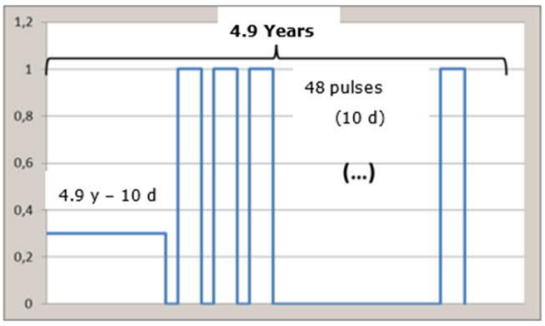

Figure 10. 1st DEMO operation phase irradiation scenario: availability 30% in the first 1800 days + 10 days with 48 pulses at 1998 MW (100%), 4 hours long with 1 hour of dwell time, derived and modified by the reference scenario [34].

The simulations have been performed using standard MCNP cell-based tallies (F4), calculating neutron spectra on the cells of interest. The results have been normalized to 1998 MW fusion power (neutron yield: 7.094×10^{20} n/s), according to the plasma parameters specified in table 1. The calculations have been performed on the ENEA CRESCO cluster [6].

Table 6. Reference tungsten composition used for neutronics analyses [18].

Tungsten	Reference for neutronics analyses
Density (g/cm^3)	19.00
Composition	wt %
W	99.9595
Ag	0.001
Al	0.0015
As	0.0005
Ba	0.0005
Ca	0.0005
Cd	0.0005
Co	0.001
Cr	0.002
Cu	0.001
Fe	0.003
K	0.001
Mg	0.0005
Mn	0.0005
Na	0.001
Nb	0.001
Ni	0.0005
Pb	0.0005
Ta	0.002
Ti	0.0005
Zn	0.0005
Zr	0.0005
Mo	0.01
C	0.003
H	0.0005
N	0.0005
O	0.002
P	0.002
S	0.0005
Si	0.002

Activation quantities have been assessed by means of FISPACT II code and considering an irradiation history showed in figure 10, which corresponds to 4.9 years operational scenario (equivalent to 1.5 FPY), and it has been derived from the reference scenario [34], and then, slightly reduced in order to adapt the time of irradiation to that, currently foreseen for the DEMO divertor.

Table 7. Tungsten – "Chinese" composition, made by AT&M company [19].

Tungsten-China	AT&M
Density (g/cm^3)	19.105
Composition	wt %
W	99.9711
Si	0.01
Ni	0.005
Fe	0.005
N	0.002
O	0.002
C	0.0049

Table 8. Tungsten – "Japanese" composition, made by A.L.M.T. company [32].

Tungsten-Japan	A.L.M.T.
Density (g/cm^3)	19.26
Composition	wt %
W	99.9959
Fe	0.0005
Ni	0.0001
Si	0.0005
C	0.001
O	0.001
N	0.001

Table 9. Chromium composition, made by Plansee company [33].

Chromium	Plansee
Density (g/cm^3)	7.15
Composition	wt %
Cr	99.89
Fe	0.03
Si	0.01
W	0.005
Mo	0.005
C	0.01
O	0.03
N	0.02

Table 10. Copper composition, made by AT&M company [19].

Copper	AT&M
Density (g/cm^3)	8.96
Composition	wt %
Cu	99.99433
S	0.0006
O	0.0003
P	0.0002
Zn	0.0001
Te	0.00001
Sn	0.0001
Se	0.0001
Sb	0.0001
Pb	0.0001
Ni	0.001
Mn	0.00005
Fe	0.001
Cd	0.0001
Bi	0.00001
As	0.0005
Ag	0.0014

3.1 Comparison between the effects of the WCLL and HCPB blanket on W activation behaviour

Poloidal profiles of specific activity (Bq/kg) on W are shown in figures 11, 12 and 13 considering the following cooling times after plasma shutdown: beginning time, 1 year and 50 years, respectively. As far as WCLL blanket is concerned, W generally shows higher activity values than HCPB case, for any cooling time.

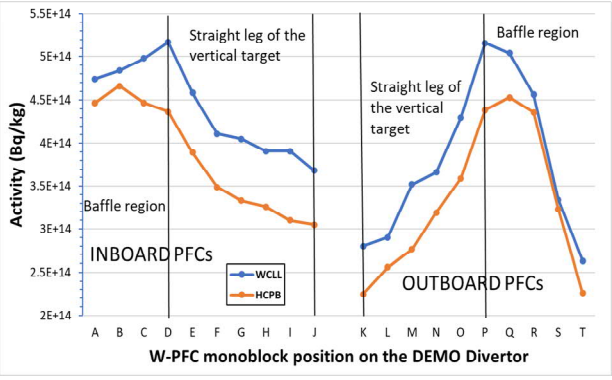

Figure 11. Comparison between the poloidal profiles of specific activity (Bq/kg) of divertor W-armour, evaluated for HCPB and WCLL blanket, on the target external side (highlighted in red in figure 3), considering the starting time after plasma shutdown.

As expected, the peak values are in the baffle region, where the monoblocks are more exposed to neutrons (at the beginning, WCLL, D and P: more than 5x10^{14} Bq/kg, HCPB, B and Q: around 4.5x10^{14} Bq/kg); there is a gradually decrease towards the lower part of the target. At the starting time, the WCLL profile shows values +20/25% greater than HCPB case. Observing figures 12 and 13, these differences are largely softened after 1 year, and even more after 50 years, highlighting ranges of variation between +5 and +10% for WCLL compared to HCPB.

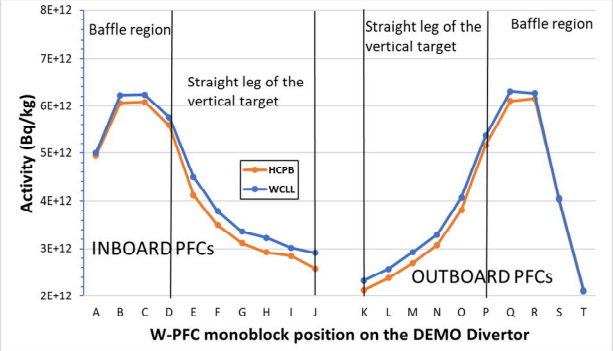

Figure 12. Comparison between the poloidal profiles of specific activity (Bq/kg) of divertor W-armour, evaluated for HCPB and WCLL blanket, on the target external side (highlighted in red in figure 3), at 1 year after plasma shutdown.

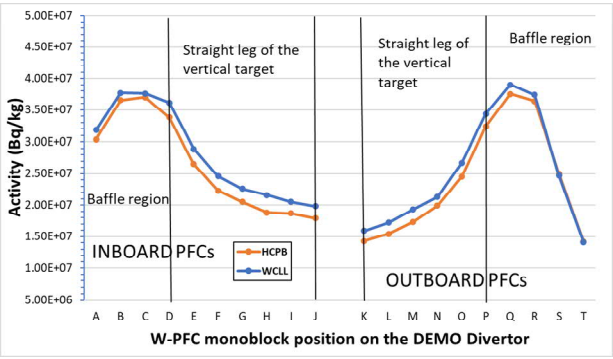

Figure 13. Comparison between the poloidal profiles of specific activity (Bq/kg) of divertor W-armour, evaluated for HCPB and WCLL blanket, on the target external side (highlighted in red in figure 3), at 50 years after plasma shutdown.

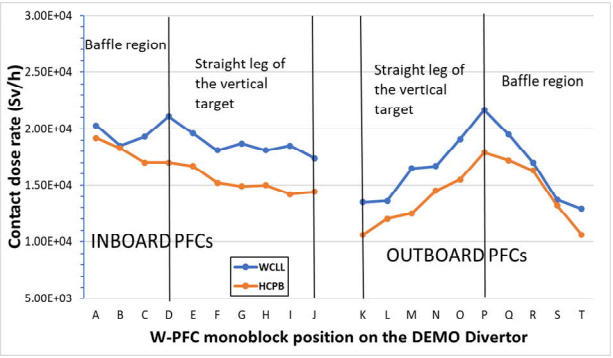

Figure 14. Comparison between the poloidal profiles of contact dose rate (Sv/h) of divertor W-armour, evaluated for HCPB and WCLL blanket, on the target external side (highlighted in red in figure 3), considering the starting time after plasma shutdown.

In figures 14, 15 and 16, poloidal profiles of contact dose rate (Sv/h) are plotted, referring to starting time, 1 year and 50 years after shutdown, respectively. In accordance with what has been stated for the activity, contact dose

shown with the water cooled blanket is generally higher than the helium cooled one, for any cooling time.

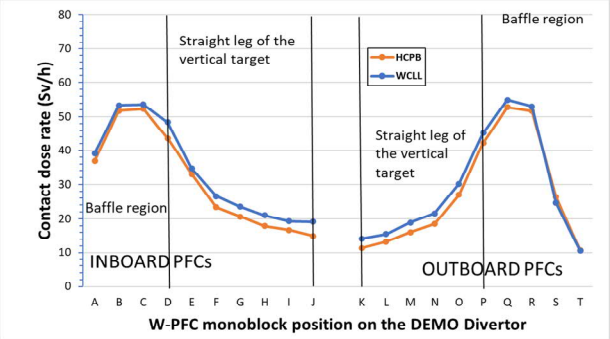

Figure 15. Comparison between the poloidal profiles of contact dose rate (Sv/h) of divertor W-armour, evaluated for HCPB and WCLL blanket, on the target external side (highlighted in red in figure 3), at 1 year after plasma shutdown.

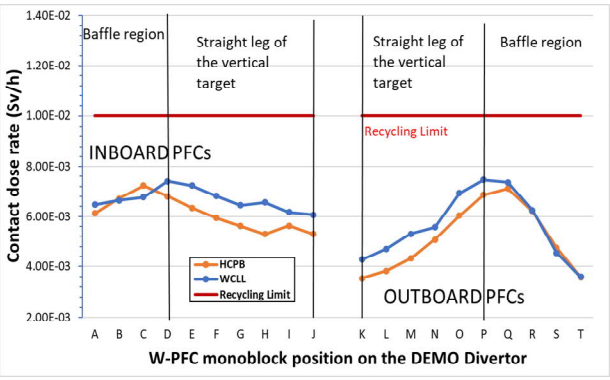

Figure 16. Comparison between the poloidal profiles of contact dose rate (Sv/h) of divertor W-armour, evaluated for HCPB and WCLL blanket, on the target external side (highlighted in red in figure 3), at 50 years after plasma shutdown.

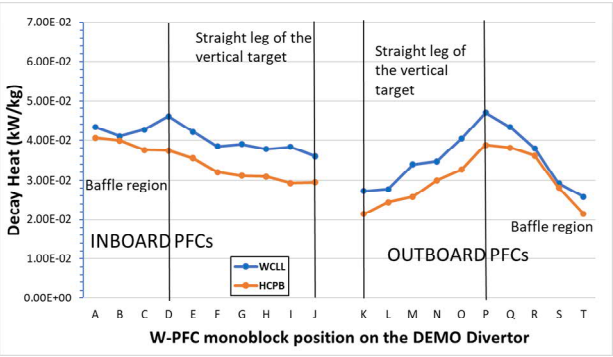

Figure 17. Comparison between the poloidal profiles of decay heat (kW/kg) of divertor W-armour, evaluated for HCPB and WCLL blanket, on the target external side (highlighted in red in figure 3), considering the starting time after plasma shutdown.

The maximum values are in the baffle region (at the beginning, WCLL, D and P: 2.2×10^4 Sv/h, HCPB, A and P: 1.9×10^4 Sv/h and 1.8×10^4 Sv/h, respectively). Again, the differences between the profiles are reduced after 1 year and 50 years. At these two cooling times, slightly higher dose levels (figures 15 and 16) for HCPB compared to WCLL in monoblocks B, C (inboard) and S, T (outboard), can be observed. If a reference value of contact dose of 10 mSv/h is considered, for the waste recycling, looking at figure 16, all the W-monoblocks, for both the blanket configurations, show doses well below than this value, suggesting that, under these conditions, it might be possible to recover these components after 50 years from the end of irradiation. Regarding the decay heat (kW/kg) poloidal profiles (figures 17, 18 and 19, starting time, 1 year and 50 years after shutdown, respectively), their trends are very similar to those already described for specific activity and contact dose.

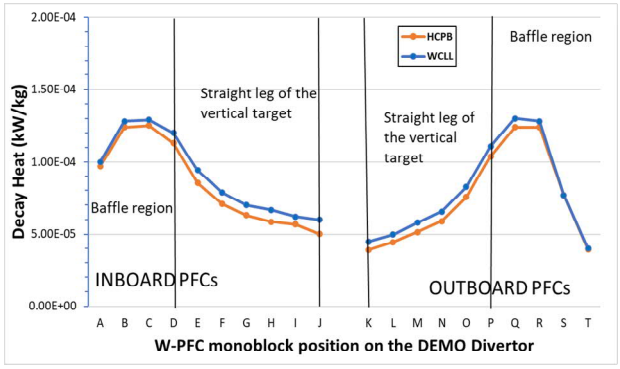

Figure 18. Comparison between the poloidal profiles of decay heat (kW/kg) of divertor W-armour, evaluated for HCPB and WCLL blanket, on the target external side (highlighted in red in figure 3), at 1 year after plasma shutdown.

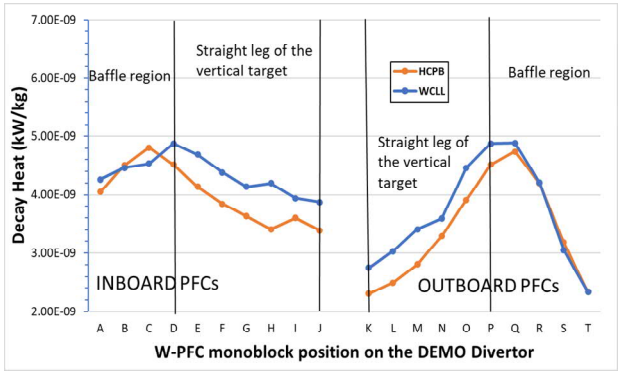

Figure 19. Comparison between the poloidal profiles of decay heat (kW/kg) of divertor W-armour, evaluated for HCPB and WCLL blanket, on the target external side (highlighted in red in figure 3), at 50 years after plasma shutdown.

The decay heat values with WCLL are basically greater than HCPB case. The peak values are in the baffle region (starting time, WCLL, D and P: circa 4.7×10^{-2} kW/kg, HCPB, A and P: 4.1×10^{-2} and 3.9×10^{-2} kW/kg, respectively). The differences between the profiles are in the order of +5/30% for WCLL, at the initial cooling time. It decreases to -4%/+15% after 1 year and 50 years, confirming the gradual reduction of the discrepancy between the profiles with increasing time. Even for the decay heat (figures 18 and 19), there are points where the HCPB shows slightly larger values than the WCLL. The W activation behaviour, underlined by means of poloidal profiles trends, plotted for different cooling times, could be preliminarily explained in the following way: they almost exactly agree with the timescale of dominance for 187W (T1/2 = 23.72 h), which is produced chiefly via (n,γ) reactions on 186W (28.43 % at. of pure W) that are most probable (have the highest reaction cross sections) at low neutron energies. The analysis suggests that the greater neutron moderation in

the water cooled blanket of the WCLL concept, results in a neutron spectrum (figure 20) with a higher proportion of low energy neutrons in the divertor W-armour than HCPB, thereby enhancing 187W production [35]. The effect of the 187W is therefore predominant for shorter cooling times, and increasingly mitigated for longer times after shutdown.

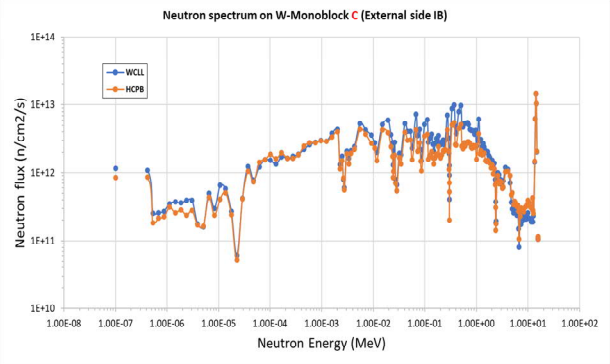

Figure 20. Comparison between the WCLL and HCPB neutron spectra impinging on the W-Monoblock, C position, external side (figure 3, red) of the inboard target (total neutron flux, WCLL: 4.06×10^{14} n/cm^2/s, HCPB: 2.96×10^{14} n/cm^2/s).

3.2 Assessment of the concentration of the main transmutation products of Tungsten and Copper

The atomic concentrations of the primary transmutation products of tungsten [18] and copper [19] have been evaluated (table 11, figures 21 and 22), considering both the blankets under analysis and two different cooling times: initial time and 1000 years after plasma shutdown. The assessment of these quantities may help to understand how the thermo-mechanical and physical properties of W and Cu, change after irradiation. Under the impact of neutron irradiation some W isotopes produce a significant transmutation to Re or Os via complex (n,γ) reactions. Neutron exposure can lead to the formation of defects (e.g. dislocation loops, voids) and it can induce precipitations and segregation of Re and Os in the microstructure [36][37][38][39], thus affecting the mechanical and thermal properties (e.g. thermal conductivity [40]) of W under neutron irradiation. The content of H and He gases (emitted from certain neutron reactions) can cause both swelling and a strong increase in brittleness. In the same time, the content of Nickel and Zinc (produced by means of complex multistep reactions, starting from 63Cu and 65Cu) has an important impact on the loss of thermal conductivity of copper and CuCrZr [41][42], affecting the PFCs heat removal capacity. Therefore, the evaluation of these quantities may help to quantify the degradation of the physical and thermo-mechanical properties of these plasma facing materials, under neutron irradiation condition DEMO relevant. Table 11 shows the expected peak values and it highlights how the concentrations of these transmutation products are substantially unchanged between the initial instant of time after plasma shutdown and the following 1000 years. These concentration values could indicatively be reached in correspondence with the PFCs placed on the baffle region and external sides of the target (series B, C, D, E and O, P, Q, R, figure 8).

Table 11. Comparison between the expected peak values of the main transmutation products (% at.) of W [18] and Cu [19] used in the divertor PFCs, considering the WCLL and HCPB blanket. These values are provided for two different cooling times: starting time after shutdown and 1000 years after shutdown.

Tungsten	WCLL % at. (staring time)	HCPB % at. (starting time)	WCLL % at. (1000 years)	HCPB % at. (1000 years)
W	98.77	98.84	98.73	98.81
Re	0.82	0.75	0.85	0.77
Os	0.05	0.04	0.05	0.04
H	0.09	0.09	0.09	0.09
He	1.5×10^{-4} % at. (starting time)	1.5×10^{-4} % at. (starting time)	1.5×10^{-4} % at. (1000 years)	1.5×10^{-4} % at. (1000 years)
Copper				
Cu	99.52	99.56	99.53	99.57
Ni	0.27	0.25	0.26	0.24
Zn	0.12	0.11	0.12	0.11

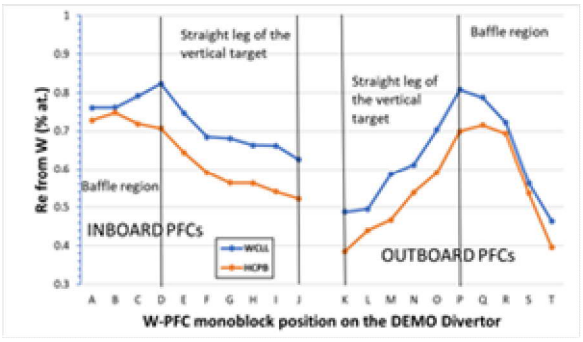

Figure 21. Comparison between the poloidal profiles of the atomic concentration (%) of Re transmuted from tungsten [18], evaluated for HCPB and WCLL blanket, on the divertor target external side (highlighted in red in figure 3), considering the starting time after plasma shutdown.

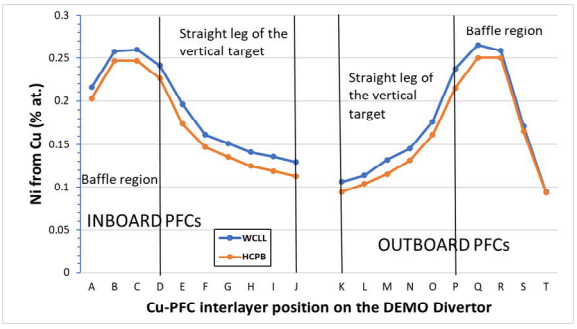

Figure 22. Comparison between the poloidal profiles of the atomic concentration (%) of Ni transmuted from copper [19], evaluated for HCPB and WCLL blanket, on the divertor target external side (highlighted in red in figure 3), considering the starting time after plasma shutdown.

This behaviour is better shown in figures 21 and 22, which highlight, respectively, the poloidal profiles along the target of the Re and Ni (transmuted from tungsten [18] and copper [19], respectively) atomic concentrations for both the blankets and in correspondence of the initial time after plasma shutdown. Although there aren't still reference limit values for these quantities, previous studies [39][43][44] have provided expected estimates, which are in line with those calculated in this analysis.

3.3 Comparison between two different Tungsten compositions (main candidates), the reference W composition and Chromium

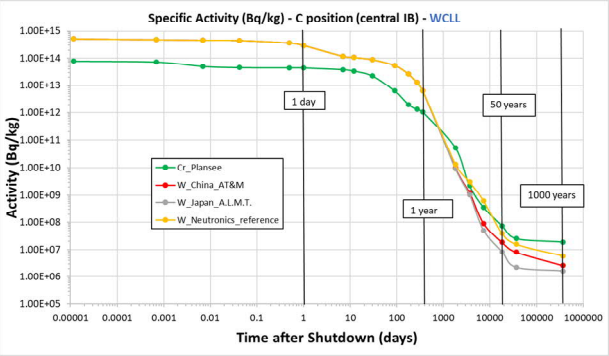

Figure 23. Comparison between the specific activity (Bq/kg) of W reference composition for neutronics study [18], W composition of AT&M Chinese [19] and A.L.M.T. corp. Japanese [32], and chromium [33].

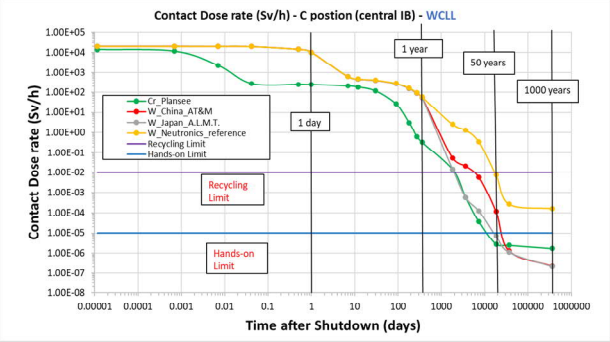

Figure 24. Comparison between the contact dose rate (Sv/h) of W reference composition for neutronics study [18], W composition of AT&M Chinese [19] and A.L.M.T. corp. Japanese [32], and chromium [33].

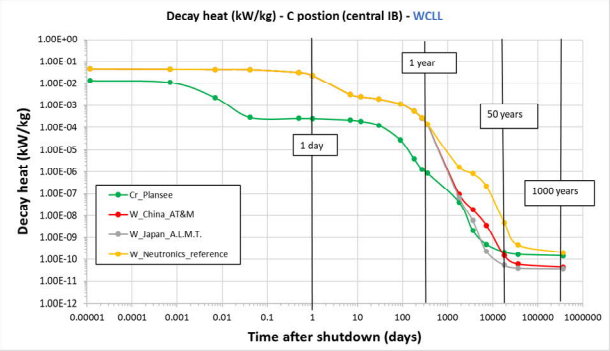

Figure 25. Comparison between decay heat (kW/kg) of W reference composition for neutronics study [18], W composition of AT&M Chinese [19] and A.L.M.T. corp. Japanese [32], and chromium [33].

Comparison between different W compositions (reference for the neutronics analyses [18], AT&M Chinese company [19], A.L.M.T. corp. Japanese company [32]) and chromium (made by Plansee company [33]), has been done, in terms cooling time profiles of specific activity, contact dose rate and decay heat (figures 23, 24 and 25 respectively). In this case, the evaluation has been carried out on the monoblock C placed in the central zone of the inboard baffle region (figure 3), referring only to the WCLL blanket case. The calculations of the neutron spectra on tungsten have been performed considering the MCNP WCLL DEMO model described in this dissertation. On the contrary, the MCNP model of chromium LA PFCs concept [15] has been implemented in the last year MCNP WCLL DEMO model [29][45], following the reference geometry. Nevertheless, the similarity between the two models and the same irradiation conditions, made it possible to compare the results. The maximum nuclear loads expected in the central zone of the baffle region amount to 20.3 W/cm^3 (nuclear heating density), 1.8 appm/FPY (Helium production) and 2 dpa/FPY (nuclear damage), as far as tungsten is concerned. Regarding chromium the following nuclear heating density, Helium production and nuclear damage level are foreseen: 6.7 W/cm^3, 41 appm/FPY and 4.3 dpa/FPY. As regards the comparison between the various compositions of tungsten and chromium, observing figures 23, 24 and 25, the following observations can be deduced:

- W Japanese and Chinese have an identical time trend after shutdown for short-medium cooling times (W effect is predominant), and small differences for longer times (from 50 years onwards), due to the fact the W Chinese contains a higher level of Ni and Fe impurities than W Japanese (tables 7 and 8).
- W composition reference used for the neutronics analysis (with a greater number and rate of impurities than the others) shows a similar behaviour compared with the other two W for short-medium times (effect of W), and increased activity, contact dose rate and decay heat for longer times (effect of impurities listed in table 6, such as N, K, Ca, Co, Nb, Ag, Ni, Fe, Al, ecc).
- Chromium confirms to be a better material than tungsten in terms of activation for short and medium cooling times (1 year), for longer times this effect is much more limited: after 5 years the difference is negligible due to impurities effect (N, table 9).

4. Conclusions

Starting from the EU DEMO1 2017 reference configuration MCNP model (representing a 11.25° toroidal sector of the tokamak) two MCNP models have been reproduced: with WCLL and HCPB Single Module Segment layered blankets, both with the MCNP model of the divertor 2019 configuration. The accurate MCNP

representations of the complete ITER-Like PFCs inboard and outboard targets have been recreated and integrated in both the above-mentioned models. A detailed and extensive comparative analysis, regarding tungsten used in the Divertor PFCs targets has been performed, mainly consisting of:

- Comparison between the effects of the Water Cooled Lithium Lead (WCLL) and Helium Cooled Pebble Bed (HCPB) blanket on W activation behaviour (Activity, contact dose rate and decay heat): inboard and outboard poloidal profiles, for different times after shutdown are provided, considering the W-Monoblocks placed on the external side of the targets, where the neutron fluxes are generally more intense, and an irradiation time of 1.5 FPY. W in WCLL case, shows generally higher activity, contact dose rate and decay heat values than HCPB blanket. The differences between profiles are more softened after 1 year and even more after 50 years. This is almost surely due to the different neutron spectrum, which shows higher fluxes at lower energy for the WCLL case (water moderation effect). The peak values are in the baffle region (B, C, Q, R positions).
- The concentrations of the main transmutation products of tungsten [18] (Re, Os, H, He) and copper [19] (Ni, Zn) have been assessed (table 11).
- Comparison between different W compositions (Chinese made by AT&M [19], Japanese made by A.L.M.T [32], reference for neutronics analyses [18]) and chromium (made by Plansee [33]): W Japanese and Chinese have an identical time trend after shutdown for short-medium cooling times and small differences for longer times (from 50 years onwards), due to the fact the W Chinese contains a higher level of Ni and Fe impurities than W Japanese. W composition reference used for the neutronics analysis shows a similar behaviour compared with the other two W for short-medium times (effect of W), and increased activity, contact dose rate and decay heat for longer times (effect of impurities which are more sizeable). Chromium confirms to have a better activation response material than tungsten for shorter and medium times (1 year), for longer times this effect is much more limited (impurities impact).

Acknowledgments

This work has been carried out within the framework of the EUROfusion Consortium and has received funding from the Euratom research and training programme 2014-2018 and 2019-2020 under grant agreement No 633053. The views and opinions expressed herein do not necessarily reflect those of the European Commission.

The computing resources and the related technical support used for this work have been provided by CRESCO/ENEAGRID High Performance Computing infrastructure and its staff [6]. CRESCO/ENEAGRID High Performance Computing infrastructure is funded by ENEA, the Italian National Agency for New Technologies, Energy and Sustainable Economic Development and by Italian and European research programmes, see http://www.cresco.enea.it/english for information.

References

[1] M. Fursdon, Report on DIV-JUS-2-CD1 Target Analysis Guidelines & Structural Integrity Assessment, EFDA_D_2PAV56, 2020 (https://idm.euro-fusion.org/?uid=2PAV56&action=get_document)

[2] M. Fursdon, Report on DIV.TAR.JUS-2-CD1 Target concepts detailed design description document, 2NVYGP, 2020 (https://idm.euro-fusion.org/?uid=2NVYGP&action=get_document)

[3] X5 MONTE CARLO TEAM, “MCNP—a general Monte Carlo N-Particle transport code: version5 user's guide”, LANL report LA-CP-03-0245, October 2005.

[4] http://www.oecd-nea.org/dbdata/jeff/jeff33/

[5] The FISPACT-II User Manual UKAEA-R(18)001 February 2018, https://fispact.ukaea.uk/

[6] G. Ponti et al., "The role of medium size facilities in the HPC ecosystem: the case of the new CRESCO4 cluster integrated in the ENEAGRID infrastructure", Proceedings of the 2014 International Conference on High Performance Computing and Simulation, HPCS 2014, art. no. 6903807, 1030-1033 (https://www.eneagrid.enea.it/papers.html).

[7] T. Donné et al., European Research Roadmap to the Realisation of Fusion Energy, ISBN 978-3-00-061152-0, November 2018.

[8] G. Federici et al., Overview of the DEMO staged design approach in Europe, Nucl. Fusion 59 (2019) 066013.

[9] J.H. You et al., Conceptual design studies for the European DEMO divertor: Rationale and first results, Fusion Engineering and Design 109–111 (2016) 1598–1603.

[10] J. H. You, E. Visca, Ch. Vorpahl, Ch. Bachmann, T. Barrett, B. Böswirth, F. Crescenzi, F. Domptail, M. Fursdon, F. Gallay, B-E. Ghidersa, H. Greuner, M. Li, A.v. Müller, J. Nicholas, J. Prokupek, J. Reiser, M. Richou, S. Roccella, European divertor target concepts for DEMO: Design rationales and high heat flux performance, Nucl. Mater. Ener. 16 (2018) 1-11.

[11] J. H. You, E. Visca, T. Barrett, B. Böswirth, F. Crescenzi, F. Domptail, G. Dose, M. Fursdon, F. Gallay, H. Greuner, K. Hunger, A. Lukenskas, A. v. Müller, M. Richou, S. Roccella, C. Vorpahl, K. Zhang, High-heat-flux technologies for the European DEMO divertor targets: State-of-the-art and a summary of the latest testing campaign, J. Nucl. Mater., in press.

[12] J. H. You, R. Villari, D. Flammini, D. Marzullo, G. Mazzone, Nuclear loads and nuclear shielding performance of EU DEMO divertor: A preliminary neutronics evaluation of two interim design options, Nucl. Mater. Ener. 23 (2020) 100745.

[13] R.G. Abernethy (2017) Predicting the performance of tungsten in a fusion environment: a literature review, Materials Science and Technology, 33:4, 388-399, DOI: 10.1080/02670836.2016.1185260.

[14] D. Terentyev, T. Khvan, J.-H. You, N. Van Steenberge, Development of chromium and chromium-tungsten alloy for the plasma facing components: application of vacuum arc melting techniques, J. Nucl. Mater. 536 (2020) 152204.

[15] F. Crescenzi et al., Final Report on Deliverable DIV-2.4.5-T001-D001 Chromium concept: 2nd Phase Design Study Report, EFDA_D_2MF5J3, 2018.

[16] J.H. You, A review on two previous divertor target concepts for DEMO: mutual impact between structural design requirements and materials performance, Nucl. Fusion 55 (2015) 113026.

[17] R. Villari and D. Flammini, https://idm.euro-fusion.org/?uid=2NV7J8

[18] U. Fischer et al, Technical Report Design Criteria, Codes and Standards ENS-1.1.5.0-NT-00-R10: Material compositions for PPPT neutronics and activation analyses, EFDA_D_2MM3A6 v1.1 (2018), (https://idm.euro-fusion.org/).

[19] http://www.atmcn.com/Subsidiary/Functional/Products/ (batch specification from supplier).

[20] F. Moro et al., Nuclear analysis of the Water cooled lithium lead DEMO reactor, Fus. Eng. Des., 160, (2020), Article number 111833.

[21] F. Moro et al., Neutronic analyses in support of the WCLL DEMO design development, Fus. Eng. Des., 136, (2018), 1260-1264.

[22] S. Noce, et al., Nuclear analysis of the single module segment WCLL DEMO, Fus. Eng. Des. 147 (2019) 111207.

[23] Francisco A. Hernández et al., Final Report on Deliverable HCPB Design Report 2018, EFDA_D_2NUTXK (https://idm.euro-fusion.org/).

[24] "TENDL-2015: TALYS-based evaluated nuclear data library", A.J. Koning, D. Rochman, J. Kopecky, J. Ch. Sublet, E. Bauge, S. Hilaire, P. Romain, B. Morillon, H. Duarte, S. van der Marck, S. Pomp, H. Sjostrand, R. Forrest, H. Henriksson, O. Cabellos, S. Goriely J. Leppanen, H. Leeb, A. Plompen and R. Mills, https://tendl.web.psi.ch/tendl_2015/tendl2015.html.

[25] C. Bachmann et al., Overview over DEMO design integration challenges and their impact on component design concepts, Fus. Eng. Des., 136, (2018), 87-95.

[26] D. Marzullo, https://idm.euro-fusion.org/?uid=2N24SN

[27] www.spaceclaim.com

[28] Y. Wu, FDS Team, CAD-based interface programs for fusion neutron transport simulation, Fus. Eng. Des., 84, (2009), 1987 – 1992.

[29] S. Noce et al., Final Report DIV-1-T006-D015 Neutronic analyses of plasma facing components of DEMO Divertor, EFDA_D_2NQWJV, 2019 https://idm.euro-fusion.org/?uid=2NQWJV&action=get_document.

[30] Pereslavtsev Pavel, https://idm.euro-fusion.org/?uid=2NFBYS

[31] M.H.H. Kolb et al., Li_4SiO_4 based breeder ceramics with Li_2TiO_3, $LiAlO_2$ and $Li_XLa_YTiO_3$ additions, part I: Fabrication, Fusion Engineering and Design 115 (2017) 39–48, doi: http://dx.doi.org/10.1016/j.fusengdes.2016.12.033.

[32] https://www.allied-material.co.jp/en/products/tungsten.html, (batch specification from supplier).

[33] https://www.plansee.com/en/materials/chromium.html

[34] U. Fischer et al., “Guidelines for Neutronic Analyses”, EFDA_D_2L8TR9, final report PMI-5.3-03 v1.7, 2018, (https://idm.euro-fusion.org/).

[35] M.R. Gilbert et al 2017 Nucl. Fusion 57 046015.

[36] M. Klimenkov et al., Microstructure of neutron irradiated tungsten and W-Re-Os alloys, 2P36N5 (https://idm.euro-fusion.org/).

[37] Duc Nguyen-Manh et al., Anomalous precipitation of Re, Os in neutron irradiated tungsten at high temperature, 2PALJP (https://idm.euro-fusion.org/).

[38] M.R. Gilbert et al Nucl. Fusion 57 (2017) 044002 (8pp), doi: https://doi.org/10.1088/1741-4326/aa5e2e.

[39] M.R. Gilbert and J.-Ch. Sublet, Nucl. Fusion 51 (2011) 043005 (13pp), doi: doi:10.1088/0029-5515/51/4/043005.

[40] M. Fuijitsuka et al., Effect of neutron irradiation on thermal diffusivity of tungsten-rhenium alloys, Journal of Nuclear Materials 283-287 (2000) 1148-1151.

[41] S.A. Fabritsiev et al., The effect of neutron irradiation on the electrical resistivity of high-strength copper alloys, Journal of Nuclear Materials 249 (1997) 239 – 249.

[42] S.A. Fabritsiev et al., Evaluation of copper alloys for fusion reactor divertor and first wall components, Journal of Nuclear Materials 233-237 (1996) 127 – 137.

[43] Li M. and Zinkle S.J. (2012) Physical and Mechanical Properties of Copper and Copper Alloys. In: Konings R.J.M., (ed.) Comprehensive Nuclear Materials, volume 4, pp. 667-690 Amsterdam: Elsevier.

[44] S.J. Zinkle and S.A. Fabritsiev, Copper Alloys for High Heat Flux Applications, Atomic and Plasma Materials Interaction Data for Fusion (supplement to Nuclear Fusion) 5 (I 994) 163-192.

[45] S. Noce et al., Nuclear analyses for the design of the ITER-Like Plasma Facing Components vertical targets of the DEMO Divertor, Fus. Eng. Des., (2020) 155.